Identification of Pilot-Vehicle Dynamics from In-Flight Tracking Data

R.A. Hess* and M.A. Mnich†
University of California, Davis, California

The increasing cost and complexity of ground simulation and flight test make it imperative that researchers and engineers maximize the amount of useful information they can obtain from these endeavors. Although the analytical techniques for identifying pilot-vehicle dynamics in well-defined flight tasks have been available for a number of years, the routine exercise of such techniques is still something of a rarity in simulation and flight test activity. The reason for this can often be traced to the fact that the effort involved in undertaking such identification often dominates the test activity itself. A nonintrusive identification program is exercised to shed light on the ability of such programs to serve as a practical tool for simulation and flight test engineers. Data from a simple but representative flight task involving an F-14 "pursuer" aircraft tracking a T-38 "target" aircraft in a 3-*g* windup turn and in level flight are used. Comparative identification results are provided by a Fourier coefficient method that requires a carefully designed and implemented input consisting of a sum of sinusoids. The least-squares results compare quite favorably with those of the Fourier technique. An example of crossover frequency regression is uncovered and discussed in light of the conditions surrounding one of the flight test configurations.

I. Introduction

THE control theory paradigm for human pilot modeling has encouraged researchers to apply techniques appropriate for the identification of inanimate servomechanisms to the problem of identifying human operator or pilot dynamics in certain well-defined tracking tasks. One early and successful example of this is the work of Ref. 1. Here McRuer and colleagues measured human pilot dynamics in a laboratory environment for a series of compensatory tracking tasks like the one shown in Fig. 1. The input for these tasks was a random-appearing sum of sinusoids, and the pilot's task was to keep a display element indicating system error e centered on an oscilloscope screen. The sum of sinusoids input allowed the ratio of appropriate spectral and cross-spectral densities necessary for pilot identification to be replaced by the ratio of the Fourier coefficients of pilot input and output signals, δ and e in Fig. 1. In general, the latter coefficients are much easier to measure than the former spectral densities.

The "crossover model" of pilot-vehicle dynamics developed in Ref. 1. implies that, in single-loop tracking in the presence of random band-limited disturbances or command signals, the combination of the pilot and vehicle transfer function can be approximated by

$$Y_p Y_c = \frac{\omega_c}{s} e^{-\tau_e s} \tag{1}$$

in a fairly broad-frequency band around the crossover frequency ω_c. The experiments of Ref. 1 also indicated that the parameters ω_c and τ_e in Eq. (1) are functions of the bandwidth of the disturbance/input and the order of the controlled element (Y_c in Fig. 1). around crossover.

The literature is replete with descriptions of techniques for the successful measurement of human operator or pilot dynamics in well-defined tracking tasks, e.g., Refs. 2-10. Some of these even involve the use of flight data. Thus, the research to be described here will shed light on the ability of a particular least-squares identification technique to serve as a practical tool for engineers involved in flight simulator validation and handling qualitites research. To be useful, the results of any such identification work must be interpreted in the framework of existing, well-accepted, and tractable analytical models. Thus, the results of the identification study described here will be interpreted in the light of the model given by Eq. (1).

II. Identification Techniques

The identification techniques to be utilized in this research have been alluded to in Sec. I, i.e., a Fourier coefficient method and a least-squares technique. The former will be called upon to provide corroborative identification results for the latter. Both will be applied to a flight task that can be effectively modeled by the single-loop system of Fig. 1.

Fourier Coefficient Method

With the input consisting of a random-appearing sum of sinusoids the transfer function of interest can be obtained as in Ref. 6.

$$Y_p Y_c = \frac{C_m(j\omega_i)}{C_e(j\omega_i)} \tag{2}$$

where C_m and C_e represent Fourier coefficients whose real and imaginary parts are defined as

$$\mathrm{Re}[C_m(j\omega_i)] = \frac{1}{T_i}\int_0^{T_i} m(t)\cdot\cos(\omega_i t)\,dt \tag{3}$$

and

$$\mathrm{Im}[C_m(j\omega_i)] = \frac{-1}{T_i}\int_0^{T_i} m(t)\cdot\sin(\omega_i t)\,dt \tag{4}$$

In implementing this technique, each constituent sine wave of the input/disturbance should have an integral number of cycles over the entire run length, and no sine wave frequency can be an integral multiple of any other. If the first require-

Received July 1, 1985; presented as Paper 85-1945 at the AIAA Guidance, Navigation and Control Conference, Snowmass, CO, Aug. 19-21, 1985; revision received March 15, 1986.

*Professor, Division of Aeronautical Science and Engineering, Department of Mechanical Engineering. Member AIAA.

†Graduate Student, Division of Aeronautical Science and Engineering, Department of Mechanical Engineering. Student Member AIAA.

ment is met, one may replace the T_f in the integrals of Eqs. (3) and (4) with the run length itself. Fulfilling the second requirement ensures a random-appearing input with an adequate number of constituent sine waves (as few as five can often suffice). Finally, the relative amplitudes of the constituent sinusoids should be selected so that the resulting signal represents inputs/disturbances that naturally occur in the task at hand. For example, in an aircraft tracking task, the sum of sinusoids might represent the effects of atmospheric turbulence that can be adequately modeled by white noise through a first- or second-order filter with a relatively low bandwidth (as compared to, say, the attitude bandwidth of the pilot-vehicle system). One can select the relative amplitudes of the sine waves to approximate such a band-limited signal in a variety of ways.[11]

Least-Squares Estimation Method

If the input/disturbance is not generated as a sum of sinusoids, the Fourier coefficient method must be eschewed for other identification techniques. One such technique has been recently implemented: the nonintrusive parameter identification program (NIPIP)[12] involves the assumption of a general parameter identification strategy (a mathematical model with undetermined coefficients) and determines the model by matching model output to the generated data using a running least-squares estimation procedure. The least-squares estimates for the unknown pilot model parameters are obtained by minimizing the sum of the squares of the errors between model output and actual measured data over the length of the tracking run. The NIPIP program is also capable of providing a sliding window in the identification run. Under this option, a data window is moved along in time, with the data at the beginning of the window being dropped as new data are added. This moving average over time is appropriate for identifying time-varying pilot behavior. Because of the nature of the task to be considered, the sliding window will not be utilized here. The reader is referred to Ref. 12 for details.

Although the vast majority of data acquisition now accomplished in simulation and flight test research is digital, the object of the identification work to be discussed here, i.e., the human pilot, is most effectively described as a continuous controller. Consider Fig. 2. The NIPIP technique (or any other least-squares algorithm using discretized data) essentially identifies a discrete transfer function $G(z)$ in the z domain as

$$G(z) = z\left[\frac{1-e^{-sT}}{s}\cdot H(s)\right] \tag{5}$$

where the term $(1-e^{-sT})/s$ represents the transfer function of the simplest data reconstruction device, i.e., a zero-order hold. Table 1 shows $G(z)$ for a variety of $H(s)$ transfer functions under the tranformation implied by Eq. (5).

It is somewhat difficult to interpret the dynamics of the continuous-pilot or pilot-vehicle transfer function from the identified model given by any of the entries of column 2 in Table 1. This problem can be circumvented, however, by taking the w' transform of the identified z-plane transfer function. The resulting w' transfer function will closely resemble that of the actual continuous-system transfer function provided the frequency range of interest is well below the sampling frequency.[13] This will certainly be the case here since the highest frequency of interest for our identification will be 16 rad/s, a factor of 5 below the sampling frequency.

III. Flight Task

The NASA Ames Dryden Flight Research Facility, in cooperation with NASA Langley Research Center, has conducted a series of flight tests to provide data for evaluation and specification of manned simulator characteristics, including the utility of analytical pilot models. The flight test data were generated from the following tasks: an F-14 "pursuer" aircraft was involved in a tail chase of a T-38 "target" aircraft in both level flight and in a 3-g windup turn at a nominal Mach number of 0.55 at an altitude of 10,000 ft with a nominal horizontal separation distance of 800 ft, as indicated in Fig. 3a. The F-14 pilot was using a gunsight reticle on a head-up display (HUD), as indicated in simplified form in Fig. 3a. The task of the F-14 pilot was to keep the reticle centered on a point midway between the twin exhausts of the T-38 aircraft throughout the run. A gun camera was utilized for data acquisition. In addition to normal disturbances such as atmospheric turbulence, the wake of the target aircraft, and pilot remnant, the reticle was driven in the pursuer aircraft x-z plane by a sum of 11 sinusoids. The frequencies and relative amplitudes of the sinusoids are shown in Table 2. The relative amplitudes were chosen to simulate atmospheric turbulence. Figure 4 is a representation of the task, including the vertical geometry definitions. The run length for data reduction purposes was 85.485 s. The sampling interval for the discretized data was 1/12 s (0.08333 s). A total of 43 runs were analyzed here. Of these, 33 were in the 3-g windup turn, with the remaining 10 in the level flight condition. Each data point was

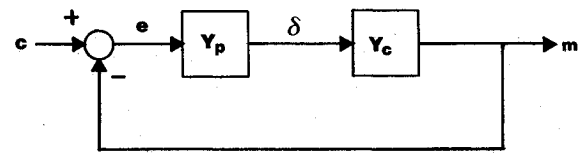

Fig. 1 Single-loop laboratory tracking task.

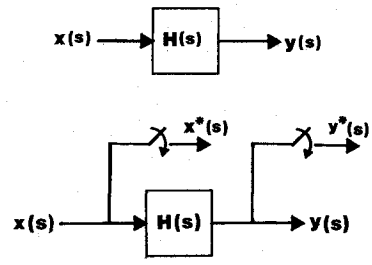

Fig. 2 Data acquisition.

Table 1 Z-plane model structures

Entry	$G(z)$	$H(s)$
1	$b_1 z^{-1}$	K
2	$\dfrac{b_1 T z^{-1}}{1-z^{-1}}$	$\dfrac{K}{s}$
3	$\dfrac{b_1 z^{-1}}{1-a_1 z^{-1}}$	$\dfrac{Ka}{s+a}$
4	$\dfrac{b_1 z^{-1}+b_2 z^{-2}}{1-a_1 z^{-1}-a_2 z^{-2}}$	$\dfrac{K\omega 2}{[\zeta;\omega]}$
5	$\dfrac{b_1 z^{-1}+b_2 z^{-2}}{1-a_1 z^{-1}-a_2 z^{-2}}$	$\dfrac{K(s+a)}{[\zeta;\omega]}$
6	$\dfrac{b_1 z^{-1}+b_2 z^{-2}}{1-a_1 z^{-1}}$	$\dfrac{K(s+a)}{(s+b)}$
7	$\dfrac{b_1 z^{-1}+b_2 z^{-2}}{1-a_1 z^{-1}-a_2 z^{-2}}$	$\dfrac{K(s+a)}{s(s+b)}$
8	$\dfrac{b_1 z^{-1}+b_2 z^{-2}+b_3 z^{-3}}{1-a_1 z^{-1}-a_2 z^{-2}-a_3 z^{-3}}$	$\dfrac{K(s+a)}{(s+b)[\zeta;\omega]}$

Table 2 Sum of sinusoids input

Frequency	No. cycles in run	Relative amplitude
0.147	2	1.17
0.442	6	0.726
0.957	13	0.293
1.399	19	0.127
1.988	27	0.0753
2.798	38	0.0457
3.976	54	0.0276
5.670	77	0.0163
7.952	108	0.00955
10.971	149	0.00592
15.978	217	0.00359

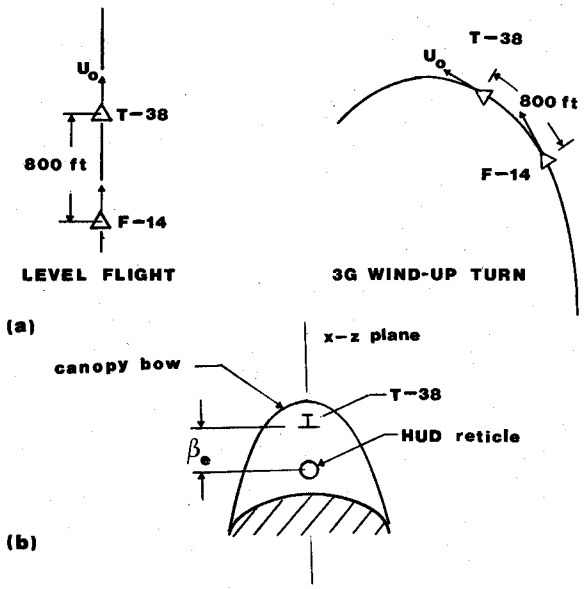

Fig. 3 a) Flight tasks, and b) F-14 HUD display.

obtained by optically scoring every other frame of the gun-camera film running at 24 frames/s. Although other variables such as control-stick motion were electrically recorded as near synchronously as possible with the film, no attempt will be made to identify transfer functions for the pilot alone (Y_p).

An analysis of the simplified geometry of Fig. 4 indicates that the transfer function between control stick δ and line of sight β can be given by

$$\frac{\beta}{\delta}(s) \simeq \frac{(s+U_0/D)}{s}\frac{\theta}{\delta}(s) - \frac{U_0}{D}\frac{1}{s}\frac{\alpha}{\delta}(s) \qquad (6)$$

Hence, θ/δ and α/δ represent the pitch-attitude-to-stick and angle-of-attack-to-stick transfer functions (including stability augmentation), and D represents to nominal separation distance (here 800 ft). Note the sign convention for β and β_e in Fig. 4.

IV. Identification Results

Simulated Data

A series of identification runs were completed on simulated data using a simplified pilot/vehicle structure as shown in Fig. 5. Reference 14 indicates that the β/δ transfer function calculated from a moving base simulator model of the F-14 in a 3-g turn closely resembles K/s in the region of probable crossover. Hence, Y_c in Fig. 5. was chosen as

$$Y_c = \frac{1}{s} \qquad (7)$$

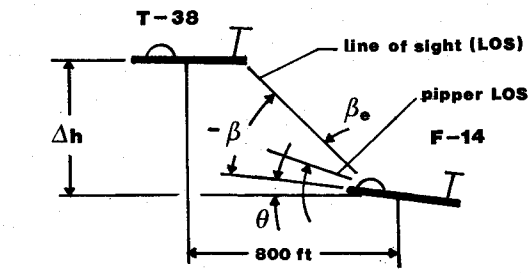

Fig. 4 Flight task geometry.

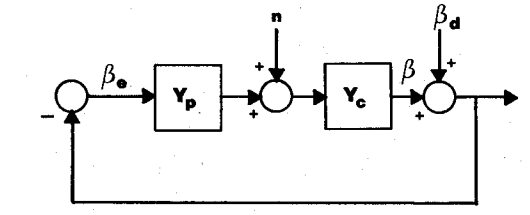

Fig. 5 Simplified pilot-vehicle structure with single noise injection.

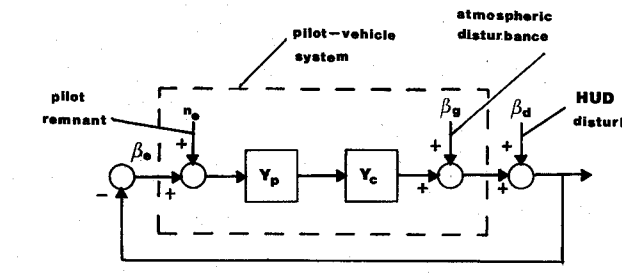

Fig. 6 Simplified pilot-vehicle structure with pilot remnant and turbulence.

The pilot transfer function Y_p was selected as

$$Y_p = \frac{2e^{-0.15s}}{(s/10)^2 + 0.04s + 1} \qquad (8)$$

A sinusoidal input identical to that intended to be exercised in the flight test was used. The Fourier coefficient and NIPIP identification techniques were applied to the problem of identifying Y_pY_c. The remaining issue is selection of the appropriate model structure from Table 1 for the NIPIP identification. It should be noted that, as implemented in NIPIP, the least-squares technique cannot identify time delays per se. However, as indicated by Table 1, delays that are integer multiples of the sampling period can be assumed in the model. The delay value then can be changed and the quality of the model fit compared for different delay values. However, the authors felt that this approach was unsatisfactory. Instead, a second-order denominator appropriate to a simple model of the human neuromuscular dynamics was included in the structure.[15] Since a substantial portion of the human pilot's effective time delay represents the low-frequency effects of higher-frequency neuromuscular dynamics[15], this approach is not unreasonable.

Entries 5 and 8 of Table 1 were selected as prospective structures for Y_pY_c. Note that entry 8 actually subsumes all lower entries in the table: i.e., by setting appropriate a_i and b_i equal to zero in the second column of entry 8, any of entries 1-7 can be obtained. Of course, in analyses such as this, there is the possibility of allowing too many degrees of freedom in the model. Such problems can be quickly identified by giving close attention to the numerical properties of the observation matrix used in the least-squares minimization procedure.[12]

Turbulence and Pilot Remnant Effects

Unmodeled atmospheric turbulence and pilot remnant can affect the identification results attempted. The injected white noise in Fig. 5 has been included to allow a brief investigation of the effects of turbulence and remnant on the control structure under study. Figure 6 shows a more complete diagram in which both pilot remnant (n_e) and turbulence (β_g) appear explicitly. One way of quantifying the effects of n_e and β_g is through the linear correlation coefficient $\rho^2(\omega)$, defined as the ratio of the linearly correlated output power spectrum to the total output spectrum.[16] A system in which $\rho^2(\omega) = 1.0$ over all frequencies can be modeled by a set of linear, constant coefficient differential (or difference) equations with arbitrary accuracy. In terms of Fig. 6, one can show

$$\rho^2(\omega) = \frac{|Y_p Y_c(j\omega)|^2 \Phi_{\beta_d\beta_d}(\omega)}{\Phi_{\beta_g\beta_g}(\omega) + |Y_p Y_c(j\omega)|^2 (\Phi_{n_e n_e}(\omega) + \Phi_{\beta_d\beta_d}(\omega))} \tag{9}$$

In addition, Fig. 6 can be used to show that the power spectral density of the error signal $\Phi_{\beta_e\beta_e}(\omega)$ can be given by

$$\Phi_{\beta_e\beta_e}(\omega) = \frac{\Phi_{\beta_d\beta_d}(\omega) + \Phi_{\beta_g\beta_g}(\omega) + |Y_p Y_c(j\omega)|^2 \Phi_{n_e n_e}(\omega)}{|1 + Y_p Y_c(j\omega)|^2} \tag{10}$$

Now the quality of the least-squares identification to be attempted will depend upon 1) selecting the appropriate $H(z)$, 2) having $\rho^2(\omega)$ close to unity over a broad frequency range $\omega_0 \le \omega \le \omega_1$, and 3) having $\Phi_{\beta_e\beta_e}(\omega)$ contain a majority of its power evenly distributed between ω_0 and ω_1. The first criterion asks that the system to be identified be parameterized by a linear model with sufficient degrees of freedom. The second asks that the system to be identified be sufficiently linear to be amenable to any linear representation such as the $H(z)$ of step 1. The third asks that the system to be identified be adequately excited over a frequency range broad enough to encompass all the modes implied by the $H(z)$ selected in step 1.

Figures 7 and 8 show the identification results for the Fourier coefficient and least-squares method for entries 5 and 8 of Table 1 with the system of Fig. 5 and with no-noise injection. Figures 9 and 10 show results for the least-squares case with injected white noise. The RMS value of the injected noise n was equal to that of the input β_d. All identification results have been interpreted in the frequency domain, and in the case of the least-squares approach, the frequency shown is defined as

$$\nu' = \frac{2}{T}\tan(\omega T/2) \tag{11}$$

Only results for frequencies less than 10 rad/s are indicated in the figures. As Figs. 7 and 8 indicate, the Fourier coefficient results match the actual simulated $Y_p Y_c$ exactly. This is to be expected. In the least-squares case, however, both models appear to be in error at the higher frequencies, with entry 5 appearing to match the simulated transfer function more closely than the entry 8 structure. Figures 9 and 10 indicate that when noise is added, the match obtained with entry 5 is degraded somewhat, while that for entry 8 is improved over the no-noise cases. One can rewrite Eqs. (9) and (10) for the case of the noise injection shown in Fig. 5 as

$$\rho^2(\omega) = \frac{|Y_p Y_c(j\omega)|^2 \Phi_{\beta_d\beta_d}(\omega)}{|Y_c(j\omega)|^2 [\Phi_{nn}(\omega) + |Y_p(j\omega)|^2 \Phi_{\beta_d\beta_d}(\omega)]} \tag{12}$$

and

$$\Phi_{\beta_e\beta_e}(\omega) = \frac{\Phi_{\beta_d\beta_d}(\omega) + |Y_c(j\omega)|^2 \Phi_{nn}(\omega)}{|1 + Y_p Y_c(j\omega)|^2} \tag{13}$$

That noise apparently degrades the quality of the transfer function fit for entry 5 while improving it for entry 8 can be explained via the three criteria mentioned below Eq. (10). First, recall that the RMS value of n is equal to that of β_d here, that n has its power equally distributed over all frequencies,

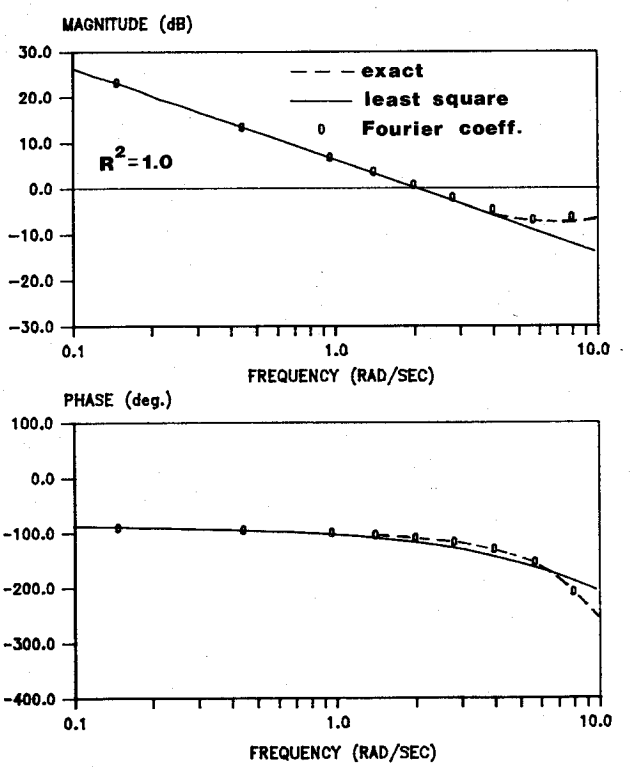

Fig. 7 Identification of simulated pilot-vehicle system of Fig. 5, entry 5, no noise injection.

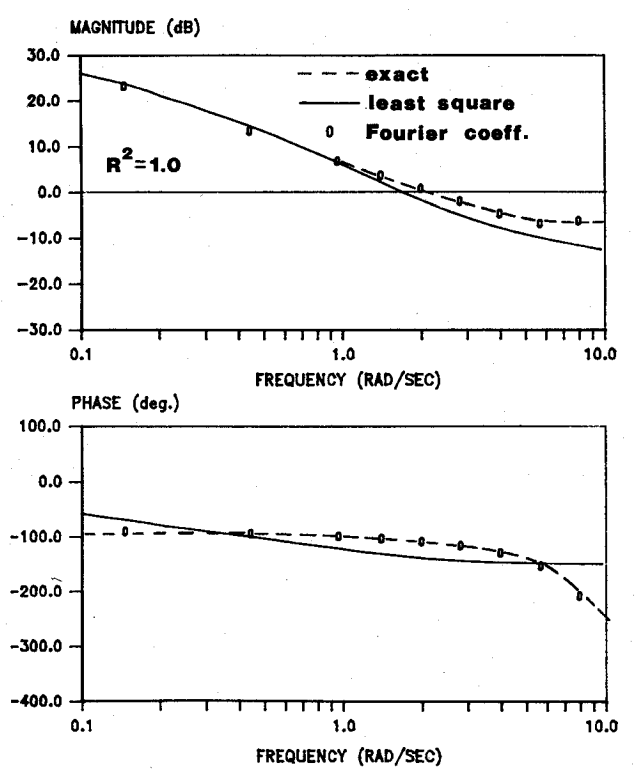

Fig. 8 Identification of simulated pilot-vehicle system of Fig. 5, entry 8, no noise injection.

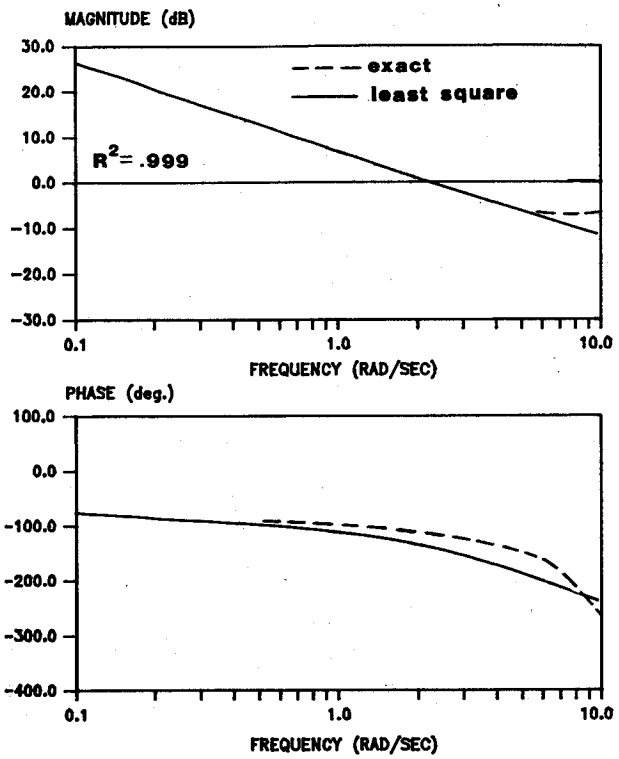

Fig. 9 Least-squares identification of simulated pilot-vehicle system of Fig. 5, entry 5, noise injection.

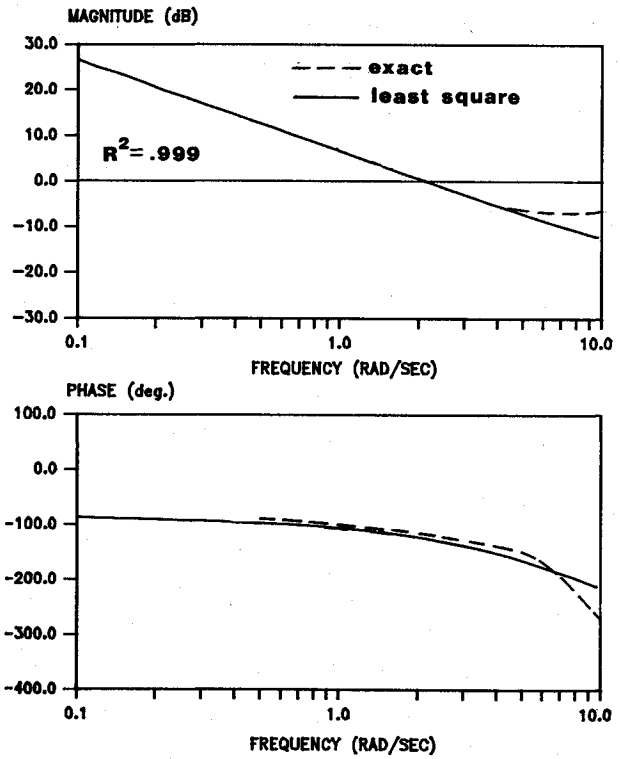

Fig. 10 Least-squares identification of simulated pilot-vehicle system of Fig. 5, entry 8, noise injection.

and the $|Y_p| > 1.0$ over a broad frequency range. This means that the noise injection will broaden the frequencies over which β_e has significant power but not influence the frequency distribution of $\rho^2(\omega)$ to as great extent. Considering the time delay in Eq. (8), entry 5 does not contain enough degrees of freedom to match the transfer function amplitude and phase characteristics at all frequencies. This is not a serious problem when no noise is present, since β_e contains most of its power at low frequencies where $\rho^2(\omega)$ is close to unity and where the phase lags due to the time delay are relatively small. When noise is added, however, Eq. (13) shows that the spectrum of β_e will be broadened and begin to encompass those frequencies where the phase lags due to the time delay are relatively large. The lack of sufficient degrees of freedom now becomes a problem as is evident in the poor phase matches of Fig. 9 as compared to Fig. 7. Entry 8 has more degrees of freedom available and can take advantage of the broadened β_e spectrum to provide a better transfer function fit. However, without noise, and with the β_d used here, the spectrum of β_e is too narrow to allow the additional degrees of freedom to be effectively utilized. In fact, as a comparison of Figs. 7 and 8 shows, entry 8 yields a poorer match than entry 5 when the least-squares fit is interpreted in the frequency domain. It may seem surprising that entry 8 does not do at least as good a job as entry 5 in the no-noise case. Actually, of course, it *does* in terms of the final value of the parameter that defines the *time-domain* least-squares procedure, i.e.,

$$R^2 = 1 - \left[\sum_{n=1}^{N} (\beta_n - \hat{\beta}_n) \Big/ \sum_{n=1}^{N} (\beta_n)^2 \right] \tag{14}$$

R^2 is also referred to as a correlation coefficient but differs from that defined in Eqs. (9) and (12). Thus, as far as the least-squares procedures goes, all the fits of Figs. 7-10 are equally good ($R^2 = 0.999$). This emphasizes the fact that the value of R^2 alone is not an adequate measure of fit quality in terms of a transfer function, as amply demonstrated by Figs. 7-10.

Flight Data

Very early in the analysis of the flight data, it became apparent that all was not well with the sum of sinusoids input driving the HUD reticle. In a Fourier (FFT) analysis of the data, the sinusoids were not found at the proper frequencies, and significant variations in the RMS value of the recorded commanded reticle motion were found. This was apparently due to a hardware problem in the drive motors moving the HUD reticle symbol. In order to salvage the data for use in calculating Fourier coefficients, the following procedure was implemented: A fast Fourier transformation of the input was conducted for each of the 43 runs. It was found that power appeared to be concentrated around specific frequencies but that the spectra did not exhibit the sharp "spikes" one would expect of sinusoids. This suggested that the technique used to generate the sinusoids allowed variation in the frequencies over the run. Thus, for each of the 43 runs, the "average" frequencies of the sinusoids were found, and only an integral number of cycles of these sinusoids were used in computing the appropriate Fourier coefficients for identification purposes. It was found that the frequencies obtained from the FFT analysis varied very little over the 43 runs but were not at the frequencies listed in Table 1. These new frequencies were (approximately) 0.18, 0.79, 1.00, 1.49, 2.49, 3.23, 5.09, and 7.00 rad/s. The fact that the last frequency is an integral multiple of the third will have minimal consequences on the results to be discussed, because its power is small. Higher-frequency "sinusoids" were found but were discarded because of the small power they contained. The seven identified frequencies adequately spanned the range of interest for pilot-vehicle identification.

Figures 11-14 show the identification results for the 3-g turn and level flight cases for $Y_p Y_c$ and entries 5 and 8 of Table 1. The figures summarize means and standard deviations of the identification work and indicate the mean value of the correlation coefficient for the NIPIP runs. The means and standard deviations of the RMS command-normalized reticle error were, for the 3-g case, 0.339 and 0.113, respectively, and for the level flight case, 0.476 and 0.205, respectively.

Table 3 Least-squares identification results

	Entry 5		Entry 8	
	3-g	Level	3-g	Level
a_1	1.50[a] (0.221)[b]	1.61 (0.125)	1.28 (0.211)	1.30 (0.119)
a_2	−0.502 (0.218)	0.611 (0.124)	0.00666 (0.218)	0.119 (0.183)
a_3	—	—	−0.288 0.138)	0.422 (0.0794)
b_1	−0.0849 (0.180)	−0.0360 (0.0497)	−0.0858 (0.160)	−0.0321 (0.0293)
b_2	0.148 (0.197)	0.0684 (0.0519)	0.119 (0.131)	0.0459 (0.0312)
b_3	—	—	0.0317 (0.107)	0.0181 (0.0374)
B	0.224 (0.327)	0.189 (0.135)	0.253 (0.361)	0.204 (0.145)

[a]Mean. [b]Standard deviation.

In addition to the model parameters evident in entries 5 and 8 of Table 1, the least-squares procedure also included a bias degree of freedom. For example, in the case of the entry 5 structure,

$$\beta_n = a_1\beta_{n-1} + a_2\beta_{n-2} + b_1\beta_{e_{n-1}} + b_2\beta_{e_{n-2}} + B \qquad (15)$$

where B represents the bias estimate. This term can account for any biases in the recorded data, nonzero "trim" conditions such as might be found in control-stick output (if it were being used), or unaccounted command inputs to the system.[12] Table 3 lists the means and standard deviations of the identified parameter values of entries 5 and 8 of Table 1 for the two flight conditions studied.

A cursory look at Figs. 11-14 indicates that the crossover model of Eq. (1) would nicely fit the data shown. Crossover frequencies in the range of 1-2 rad/s are in evidence as are equivalent time delays of approximately 0.2 s. As the correlation coefficient values indicate, the least-squares models provided excellent matches to the data. The phase comparison between the least-squares and Fourier coefficient results are excellent; however, the amplitude results differ at frequencies beyond crossover. The amplitude discrepancies are somewhat similar to those seen in the analysis of the simulated data in Figs. 7 and 8. It is worth emphasizing again that the command input exhibited very little power at these frequencies and that the smallest of the average correlation coefficients has a value of nearly unity. These facts suggest that the Fourier coefficient technique may actually be measuring the inverse of the transfer function of the feedback element (−1.0) at these higher frequencies.[17] Here the least-squares technique is relatively immune to this problem, since the model parameters are determined by data at frequencies at which β_e contains the majority of its power. Given these facts and the "non-sinusoidal" nature of the sinusodal input, we feel that the comparisons of Figs. 11-14 are excellent.

One qualitative result evident in the data is worthy of comment. This is the crossover frequency regression exhibited in the case of the level flight condition. Both Fourier and least-squares results indicate this. As an example of quantifying this result, consider the entry 8 data. The mean crossover frequency for the 3-g case is 1.71 rad/s, while for the level flight case it is 1.18 rad/s. An analysis of all the data (i.e., the crossover frequencies of the individual open-loop transfer functions Y_pY_c identified by NIPIP for entry 8) indicates that the differences in the mean crossover frequencies are

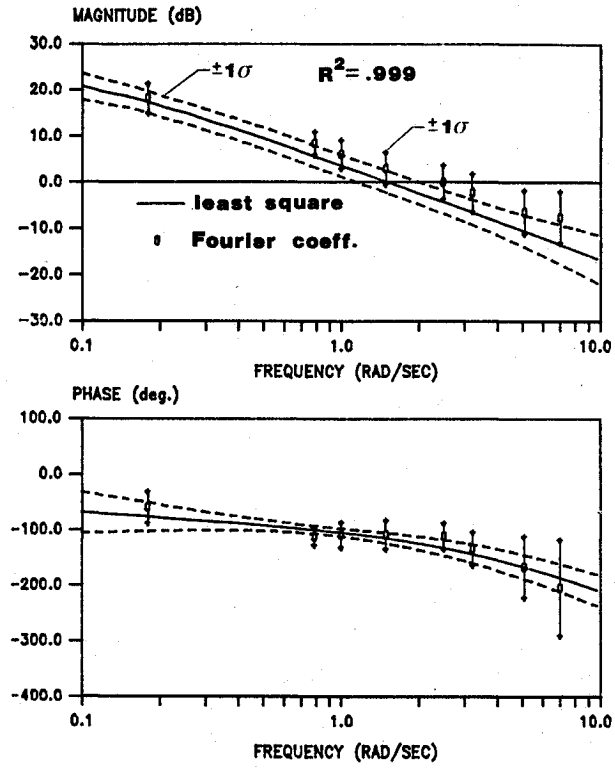

Fig. 11 Identification of F-14 pilot-vehicle system, 3-g turn, entry 5.

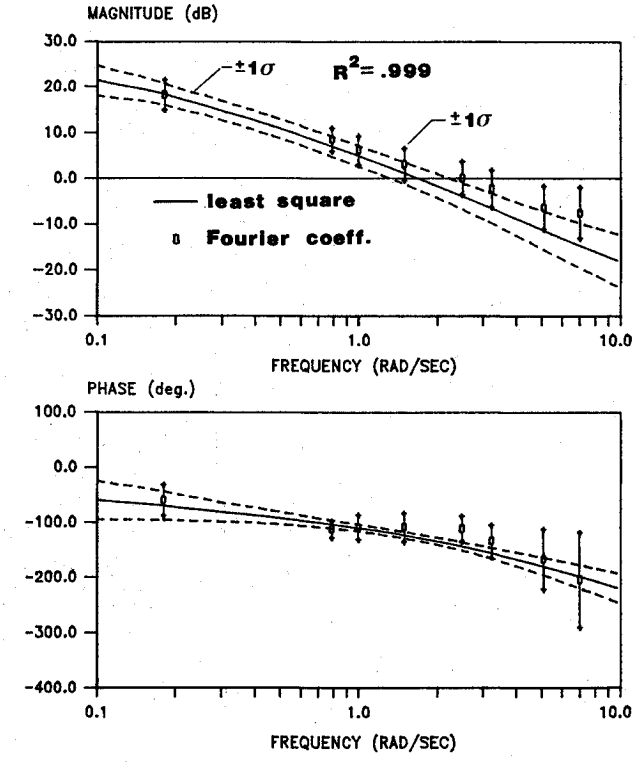

Fig. 12 Identification of F-14 pilot-vehicle system, 3-g turn, entry 8.

statistically significant at the $p = 0.0075$ level using a Wilcoxon's sum of ranks test.[18] This difference should not be overlooked since crossover frequency is perhaps the single most important pilot-vehicle parameter one can measure. For example, in manned simulation, values of ω_c significantly below those suggested by man/machine capabilities and task demands strongly suggest a lack of simulator fidelity. This may be due to a variety of causes ranging from inadequate

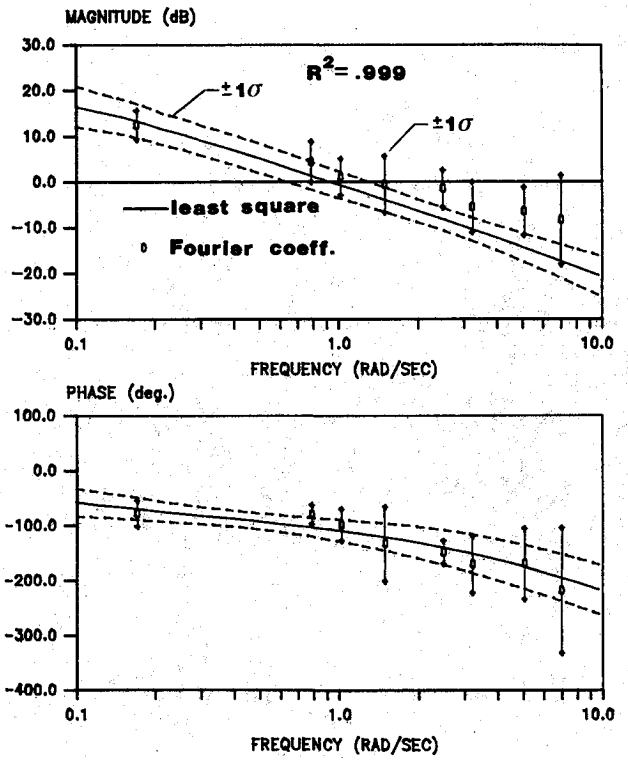

Fig. 13 Identification of F-14 pilot-vehicle system, level flight, entry 5.

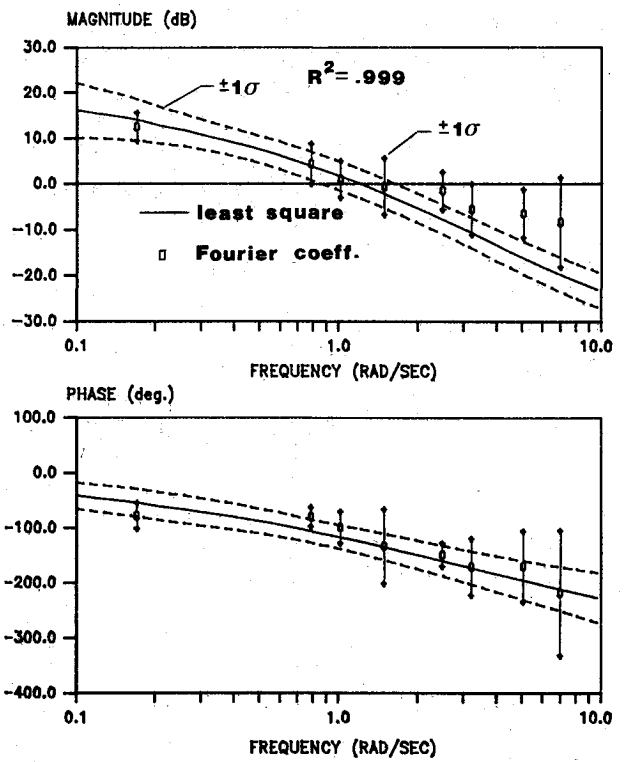

Fig. 14 Identification of F-14 pilot-vehicle system, level flight, entry 8.

motion or visual cues to the presence of time delays in the simulation.[19] In flight test, similar ω_c regression may be indicative of a vehicle susceptible to pilot-induced oscillations.[20] In the case of the task studied here, however, the cause of the regression was not nearly so portentous. Pilot comments indicated that the chase F-14 aircraft was being strongly affected by the wake of the target T-38 in the level flight condition when the HUD reticle motion yielded an F-14 flight path considerably below the target vehicle. The F-14 pilot found precision tracking extremely difficult in the presence of this disturbance and effectively reduced his gain. This type of crossover regression is "classic" since it was evident in some of the data of Ref. 1 used to generate the crossover model of the pilot. In the case of the 3-g windup turn, the decreasing radius flight trajectory minimized this interference, and crossover frequency values were not affected. The tracking performance data summarized in the paragraph above Eq. (15) corroborate this result.

V. Conclusions

Based on the research described, the following conclusions can be drawn:

1) A "nonintrusive" pilot-vehicle identification technique can be incorporated into routine flight tests involving well-defined piloting tasks.

2) Expressing identification results in the frequency (w') domain allows immediate interpretation within the framework of well-estabilished and tractable analytical models such as the crossover model of pilot-vehicle systems.

3) The least-squares technique was able to "track" a fundamental pilot-vehicle parameter such as crossover frequency and to detect wake-induced crossover frequency regression.

4) Time delay identification should be made an intrinsic part of the least-squares procedures. The delay should not be limited to integral multiples of the digital sampling interval.

Acknowledgments

This work was supported by a Postbaccalaureate Grant through the Pilot/Vehicle Dynamics Section of the Dynamics and Controls Branch of NASA Ames Dryden Flight Research Facility. The guidance of Mr. Donald T. Berry and the assistance of Mr. Peter C. Carr of that branch are gratefully acknowledged.

References

[1]McRuer, D. T., Graham, D., Krendel, E., and Reisener, W. Jr., "Human Pilot Dynamics in Compensatory Systems," Air Force Flight Dynamics Laboratory, AFFDL-TR-65-15, 1965.

[2]Elkind, J. I. and Green, D. M., "Measurement of Time-Varying and Nonlinear Dynamic Characteristics of Human Pilots," Air Force Aeronautical Systems Div., ASD TR-61-225, 1961.

[3]Bekey, G. A., Meissinger, H. F., and Rose, R.E., "A Study of Model Matching Techniques for the Determination of Parameters in Human Pilot Models," NASA CR-143, 1965.

[4]Stapleford, R. L., Craig, S. J., and Tennant, J. A., "Measurement of Pilot Describing Functions in Single-Controller Multiloop Tasks," NASA CR-1238, 1969.

[5]Wingrove, R. C. and Edwards, F. G., "Measurement of Pilot Describing Functions from Flight Test Data with an Example from Gemini X," *IEEE Transactions on Man-Machine Systems*, MMS-9, Sept. 1968, pp. 49-55.

[6]Shirley, R. S., "A Comparison of Techniques for Measuring Human Operator Frequency Response," *Proceedings of the Sixth Annual Conference on Manual Control*, 1970, pp. 803-870.

[7]Mooij, H. A., "In-Flight Measured Human Pilot Describig Functions and Remnant for Pitch Attitude Control," *Proceedings of the Ninth Annual Conference on Manual Control*, 1973, pp. 311-317.

[8]Shinners, S. M., "Modeling of Human Operator Performance Utilizing Time Series Analysis," *IEEE Transactions on Systems, Man and Cybernetics*, Vol. SMC-4, Sept. 1974, pp. 446-458.

[9]Goto, N., "A Statistical Method Applied to Pilot Behavior Analysis in Multiloop Systems," *Journal of Guidance and Control*, Vol. 3, Jan.-Feb. 1980, pp. 62-68.

[10]Biezad, D. J. and Schmidt, D. K., "Normalized Predicitive Deconvolution: A Time Series Algorithm for Modeling Human Operator Dynamics," *Journal of Guidance, Control, and Dynamics*, Vol. 8, Nov.-Dec. 1985, pp. 768-776.

[11]Junker, A. M. and Levison, W. H., "Some Empirical Techniques for Human Operator Performance Measurement," *Proceedings of*

the International Conference on Cybernetics and Society, 1980, pp. 101-105.

[12]Hanson, G. D. and Jewell, W. F., "Non-Intrusive Parameter Identification Procedure User's Guide," NASA CR-170398, 1983.

[13]Whitbeck, R. F. and Hoffman, L. G., "Digital Control Law Synthesis in the *w'* Domain," *Journal of Guidance and Control,* Vol. 1, Sept.-Oct. 1978, pp. 319-326.

[14]Baron, S. and Levison, W. H., "F-14 Modeling Study," NASA CR-172336, 1984.

[15]McRuer, D. T. and Krendel, E., "Mathematical Models of Human Pilot Behavior," AGARDograph No. 188, 1974.

[16]Graham, D. and McRuer, D., *Analysis of Nonlinear Control Systems,* Dover Publications, New York, 1971.

[17]Wingrove, R. C. and Edwards, F. G., "A Technique for Identifying Pilot Describing Functions from Routine Flight-Test Records," NASA TN D-5127, 1969.

[18]Langley, R., *Practical Statistics,* Dover Publications, New York, Chap. 6, 1971.

[19]Hess, R. A., "The Effects of Time Delays on Systems Subject to Manual Control," *Journal of Guidance, Control, and Dynamics,* Vol. 7, July-Aug. 1984. pp. 416-421.

[20]Hess, R. A., "An Analysis of Aircraft Attitude Control Systems Prone to Pilot Induced Oscillations," *Journal of Guidance, Control, and Dynamics,*" Vol. 7, Jan.-Feb. 1984, pp. 106-112.